Yang *et al.*
Protection and Control of Modern Power Systems (2023) 8:58
https://doi.org/10.1186/s41601-023-00334-6

Protection and Control of Modern Power Systems

ORIGINAL RESEARCH

Open Access

Tracking-dispatch of a combined wind-storage system based on model predictive control and two-layer fuzzy control strategy

Jingyu Yang[1,2*], Tongguang Yang[2], Longfu Luo[1] and Li Peng[2]

Abstract

To maximize improving the tracking wind power output plan and the service life of energy storage systems (ESS), a control strategy is proposed for ESS to track wind power planning output based on model prediction and two-layer fuzzy control. First, based on model predictive control, a model with deviations of grid-connected power from the planned output and the minimum deviation of the remaining capacity of the ESS from the ideal value is established as the target. Then, when the grid-connected power exceeds the allowable deviation band of tracking, the weight coefficients in the objective function are adjusted by introducing the first layer of fuzzy control rules, combining the state of charge (SOC) of the ESS with the dynamic tracking demand of the planned value of wind power. When the grid-connected power is within the tracking allowable deviation band, the second layer of fuzzy control rules is used to correct the charging and discharging power of the ESS to improve its ability to track the future planned deviation while not crossing the limit. By repeatedly correcting the charging and discharging power of the ESS, its safe operation and the multitasking execution of the wind power plan output tracking target are ensured. Finally, taking actual data from a wind farm as an example, tests on a simulation platform of a combined wind-storage power generation system verify the feasibility and superiority of the proposed control strategy.

Keywords Wind power, Energy storage system, Track planned output, Model predictive control, Two-layer fuzzy control

1 Introduction

Development of wind power is an effective way to accelerate the construction of a clean, low-carbon, safe, and efficient energy system, and to achieve sustainable energy development and dual-carbon goals [1, 2]. However, the fluctuating and intermittent nature of wind power impacts on the safe and stable operation of power grids [3–5]. Power generation plans based on short-term wind forecasts can stabilize the impact of variable wind power integration to a certain extent, but there are still large deviations between short-term forecast power and actual wind power [6, 7]. Energy storage systems (ESS) can effectively compensate for the drawbacks of wind power generation and improve the tracking accuracy of wind-storage co-generation systems for planned power output [8, 9]. However, the tracking accuracy of ESS is limited by their service life, capacity, and control mechanisms [10–13]. Given these limitations, it is critical to study the optimal control strategies for wind-storage systems [14, 15].

Many in-depth studies have looked at applying ESS in tracking the output of wind power plans [16–22]. Energy storage improves the output of wind farm tracking and power generation through either post hoc real-time section or real-time advance optimization control. Under

*Correspondence:
Jingyu Yang
yangjy8@hnu.edu.cn
[1] School of Electrical & Information Engineering, Hunan University, Changsha 410000, China
[2] Key Laboratory Energy Monitoring and Edge Computing of for Smart City of Hunan Province(Hunan City University), Yiyang 413000, China

real-time section control, the ESS corrects the deviation between the actual wind power and the planned value at each moment in real-time.

Reference [23] studies the use of ESS in a wind farm to track short-term planned output to improve wind farm tracking ability. In [24], an ESS control strategy containing five control coefficients is established and a particle swarm optimization algorithm is used to optimize and correct the charge and discharge control coefficients at each time in real-time. This improves the ability to control the ESS and track wind power planning. Reference [25] proposes a coordinated optimization control strategy combining online rolling optimization and real-time active power control. These reduce the number of energy storage charge and discharge conversions, and show improved ability to track planned output. Real-time section control adopts timely regulation without considering the future changes in the SOC of ESS batteries, while the control effect and economy of a wind-storage system are affected by battery overcharge, over-discharge, and capacity under-utilization.

The combination of real-time lead optimization control with ultra-short-term wind power prediction can achieve forward-looking lead control. Reference [12] proposes energy storage SOC feedback control based on ultra-short-term wind power prediction and scenario analysis in order to reduce the number of energy storage commands and avoid excessive charging and discharging. In [26], an optimization model is constructed to reduce the fluctuation range and the charge and discharge depth of energy storage SOC. This model, combined with wind power prediction information, adopts real-time rolling optimization to track the generation schedule and use the full ESS capacity. In [27], ultra-short-term power prediction is used to minimize the ordered times of energy storage, while advance rolling optimization is realized in the assessment period. This improves the precision of a wind power tracking plan. In [28], the Kalman filter algorithm is used to enhance the minute level of ultra-short-term wind power prediction data so as to improve the fine-grained power prediction. The algorithm, when combined with advanced rolling optimization, can accurately optimize the wind-storage system's power assessment and energy storage life. However, the effect of real-time advanced optimization control depends heavily on the accuracy of wind power prediction.

The model predictive control (MPC) algorithm has good robustness and anti-interference ability, and can better solve optimal control problems with a variety of uncertainties. A two-stage stochastic MPC with the aim of determining the optimal ESS size is proposed in [29], whereas a new control strategy based on the MPC method to fulfill the committed energy production of wind farms is presented in [30]. However, the service life of the ESS is neglected. References [31, 32] apply MPC to wind-storage systems and propose tracking scheduling instructions and minimizing energy storage output as control objectives. This improves the ability to schedule wind farm production. However, fixed values are used for the objective function weighting factors while no method is given for determining the weighting factors. In fact, the selection of weighting factors has a significant impact on MPC [33–35]. In the reviewed publications, MPC is used to determine the optimal ESS size and scheduling with the aim of reducing wind power forecast error. However, there is little research on improving the tracking capability of a wind-storage system for future planned curve by optimizing the current residual capacity of ESS in advance.

Thus, it is clear that there is a lack of comprehensive consideration of wind power prediction error and uncertainty of energy storage SOC on future tracking accuracy, and that further research is needed on how to effectively balance the contradiction between ESS lifetime and wind power plan tracking capability. Therefore, this paper proposes a combined wind-storage system tracking wind power plan control strategy based on MPC and double-layer fuzzy control, with the aim of improving both the wind-storage system tracking plan output and the ESS service life. The main contributions of this study can be summarized as:

(1) An ESS tracking wind power plan control model is established based on the MPC method. An objective function is proposed to minimize the deviation of grid-connected power from the planned output and the deviation of ESS remaining capacity from the ideal value. Consequently, the deviation of grid-connected power from the planned curve is reduced, while the ESS lifetime is taken into account.
(2) When the grid-connected power exceeds the tracking allowable deviation band, a method of using the first layer of fuzzy controller is proposed to correct the weight coefficients of the objective function to effectively resolve the contradiction between the deviations from the wind power plan and the energy storage overrun limit. The proposed method reduces the dead time and extends the service life of the ESS while improving the tracking of the planned curve.
(3) Statistical factor analysis theory is used to construct the contradictory factors between the two variables of ESS off-limit power and planned power deviation in the future optimization period. When the grid-connected power is within the tracking allowable

deviation band, a method of using the second layer of fuzzy control rules is used to correct the charging and discharging power of the ESS. Charging and discharging are carried out in advance to improve the ESS's ability to track deviations from the future plan.

A simulation platform is developed for a combined wind-storage power generation system, and the effectiveness of the proposed control strategy is verified considering a wind farm's actual operating data. The rest of this paper is organized as follows: Sect. 2 describes the topology of the combined wind-storage generation system and the creation of allowable deviation bands for generation schedule tracking. In Sect. 3, the ESS tracking wind power planning control model is established based on the MPC method, while in Sect. 4, a two-layer fuzzy control strategy is proposed. Case studies are presented in Sect. 5, and Sect. 6 concludes the paper.

2 Wind-storage co-generation system

Uncertain changes in wind speed lead to weak dispatchability of wind farm active power output. This increases the operational risk to the grid. The ability to schedule power production at a wind farm can be effectively improved by controlling the ESS charging and discharging power at the wind farm connection point. The topology of the wind-storage co-generation system is shown in Fig. 1. It mainly consists of a wind farm, an energy storage station, step-up transformers, converters, and an energy management system. These are connected to the main grid through transmission lines.

During actual grid dispatching, the power generation plan value P_p is formulated according to the wind power prediction value. The charging and discharging power

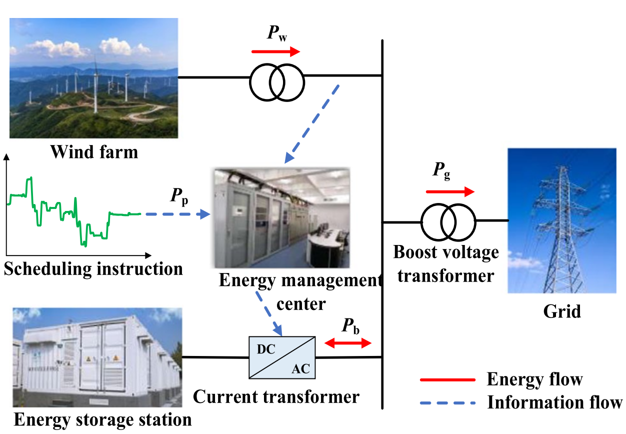

Fig. 1 Schematic diagram of the structure of a wind-storage co-generation system

P_b of the ESS is calculated through a suitable control strategy to compensate for the difference between the actual P_w and planned P_p wind power. Finally, the grid-connected power P_g of the wind-storage co-generation system is obtained. The power balance equation of the wind-storage co-generation system is:

$$P_g = P_b + P_w \tag{1}$$

For the forecasting of continuous states, in terms of mathematical solution, the time is usually discretized equally. Therefore, Eq. (1) is discretized to:

$$P_g(i+1) = P_b(i) + P_w(i) \tag{2}$$

where $P_b(i)$ and $P_w(i)$ are the power of the ESS and the actual power of the wind power at the current moment, respectively. $P_g(i+1)$ denotes the power of wind-storage co-generation system at the next moment. When $P_b(i) > 0$, the ESS is charged and when $P_b(i) < 0$, the ESS is discharged.

The iterative equation for the State of Energy (SOE) after discretization is:

$$C_{SOE}(i+1) = C_{SOE}(i) - \eta P_b(i) \times T_c / C_{rated} \tag{3}$$

where $C_{SOE}(i)$ denotes the residual ESS capacity at time i, and T_c and C_{rated} are the ESS control period and capacity, respectively. η is the ESS conversion efficiency.

According to the "Technical Regulations for Wind Power Forecasting" issued by the National Energy Administration in 2019 [36], the short-term forecast accuracy rate should be greater than or equal to 80%. Thus, the allowable deviation band of generation plan tracking, i.e., the allowable error ranges between the actual power and the planned output curve, can be written [37] as:

$$P_u(i) = (1+\delta)P_p(i) \tag{4}$$

$$P_d(i) = (1-\delta)P_p(i) \tag{5}$$

where $P_u(i)$ and $P_d(i)$ are the upper limit and lower limit of the allowable deviation band, respectively. δ denotes the deviation band set coefficient, and $P_p(i)$ refers to the planned value of wind power at time i.

The target is for the output from the combined wind-storage power generation system to be within the planned range. As shown in Area I of Fig. 2, the ESS does not act when the actual power of the wind farm is within the allowable range. When the actual power exceeds the upper limit or lower limit of the deviation band and reaches Area II, the combined output of the wind and storage at the moment is controlled within Area I via the ESS by absorbing or releasing power.

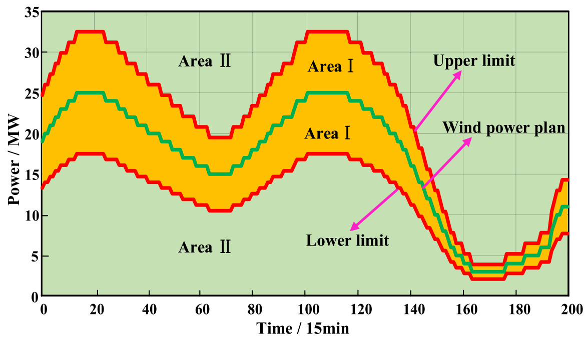

Fig. 2 Schematic diagram of the allowable deviation band for generation schedule tracking

According to the above analysis, the target power $P_a(i)$ can be calculated as follows:

$$P_a(i) = \begin{cases} P_u(i) & P_w(i) \geq P_u(i) \\ P_p(i) & P_d(i) < P_w(i) < P_u(i) \\ P_d(i) & P_w(i) \leq P_d(i) \end{cases} \tag{6}$$

3 Control model of MPC energy storage system

Based on the above power balancing equation and SOE iteration equation, the MPC system model is created. Meanwhile, the MPC rolling optimization objective function and constraints are established by combining the target power sources, taking into account the energy storage lifetime and tracking capability, and transforming the power into a quadratic programming problem for solution.

3.1 Based on MPC system model

MPC is a class of methods that consider open-loop optimal control in a finite-time domain, using the idea of rolling planning and advance control. The MPC for tracking the planned wind power output is shown in Fig. 3. At its core lies the time-domain rolling optimization process:

(1) Establish the objective function and constraints.
(2) Solve the optimization problem with constraints to obtain a sequence of control instructions for a future period using the values of state variables at the current moment.
(3) Apply the 1st value of the control instruction sequence to the control system.
(4) Scroll to the next moment and update the state variables to repeat the above process.

The schematic block diagram of the tracking plan with MPC is shown in Fig. 4. The MPC conducts real-time rolling optimization for system control. This is comprised of three parts: a prediction model, rolling optimization, and feedback correction.

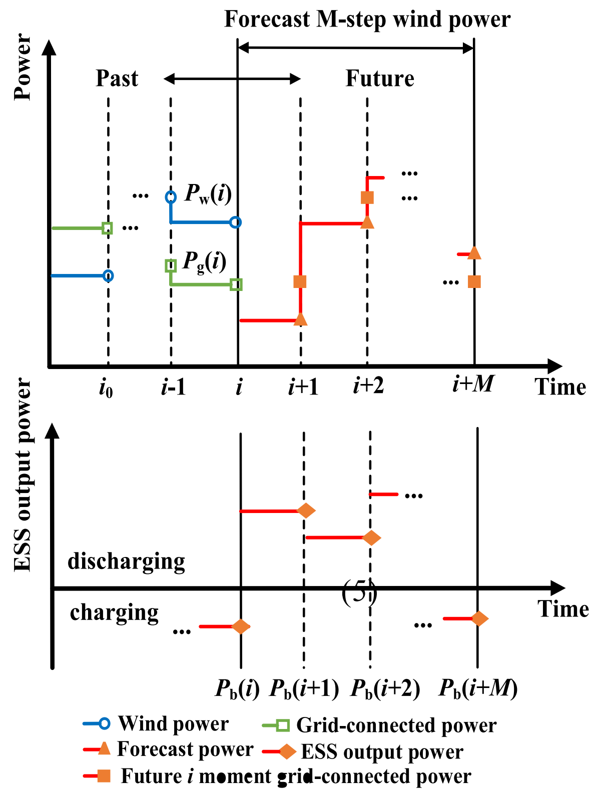

Fig. 3 MPC time domain rolling optimization process

The prediction model plays a fundamental role in model predictive control as it anticipates the future dynamic behavior of the system. Such a model relies on historical data and the current status of the system, incorporating future time domain system change trends and the impact of control instructions to forecast the system's dynamic behavior within a limited future time span.

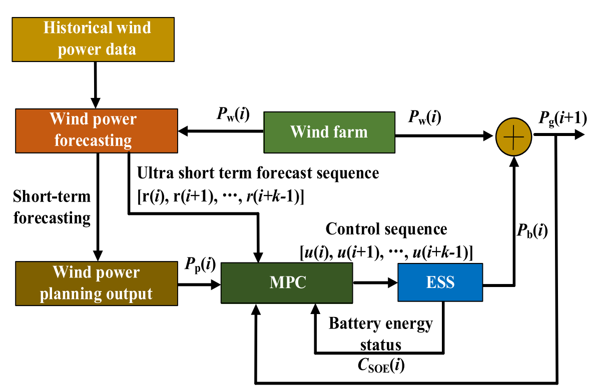

Fig. 4 MPC block diagram for tracking planned wind power output

These prediction outcomes serve as inputs for the rolling optimization stage. Here, under the influence of specific optimization objectives, the control sequence that aligns the system's predicted trend most effectively with the optimization problem requirements is considered as the optimal control instruction.

Rolling optimization serves as the central element of MPC. Its core concept involves continuously integrating system prediction information and control sequences within a limited time window to perform real-time optimization based on the specific goals defined for the controlled system. The results obtained from this process are then used to guide the system's future outputs. At each time step, the initial component of the optimal control sequence that brings the system closest to the defined optimization goal is selected as the control input for the upcoming moment. Subsequently, the new measurements generated by the system at that moment refresh the initial state of the controlled system, and the cycle repeats itself through model prediction and rolling optimization. As time progresses, the prediction time horizon also advances until the desired control objective is achieved.

In each step, MPC uses the initial element of the previously solved optimal control sequence from the prior moment to interact with the system, yielding new system state information and outputs. This process effectively refreshes the rolling optimization problem. During this process, MPC establishes both feedforward and feedback components. On the one hand, the newly acquired system state information and the ongoing system prediction information at each time step are used as inputs for the feedforward component. If any changes are detected, they are fed back into the prediction model, enabling the re-computation of the optimal control sequence through rolling optimization, thus achieving feedforward correction. On the other hand, because feedforward control has limitations in addressing existing system errors, MPC introduces a feedback loop by inputting the discrepancy between the actual system output and the predicted output at each time step into the feedback component. This creates a closed-loop system, allowing for feedback correction of the overall prediction error at that moment. This feedback mechanism enhances the robustness of the control strategy by addressing deviations that may have occurred.

From (2) and (3) and combined with the superposition theorem, the grid-connected power $P_g(i)$ and the ESS residual capacity $C_{SOE}(i)$ are selected to form the state variables, which are $\boldsymbol{x}(i)=[P_g(i),C_{SOE}(i)]^T$. The ESS output $P_b(i)$ is used as the control variable in the form of $\boldsymbol{u}(i)=P_b(i)$, while the ultra-short-term wind power $P_f(i)$ is used as an input variable as $\boldsymbol{r}(i)=P_f(i)$. The ESS $P_g(i)$ and $C_{SOE}(i)$ are selected as the output variables as $\boldsymbol{y}(i)=[P_g(i),C_{SOE}(i)]^T$. Then the state space equation of the wind-storage co-generation system is:

$$\begin{cases} \boldsymbol{x}(i+1)=\boldsymbol{A}\boldsymbol{x}(i)+\boldsymbol{B}_1 u(i)+\boldsymbol{B}_2 r(i) \\ \boldsymbol{y}(i)=\boldsymbol{C}\boldsymbol{x}(i) \end{cases} \tag{7}$$

where $\boldsymbol{A}=\begin{bmatrix} 0 & 0 \\ 0 & 1 \end{bmatrix}$, $\boldsymbol{B}_1=\begin{bmatrix} 1 \\ -\eta T_c/C_{rated} \end{bmatrix}$, $\boldsymbol{B}_2=\begin{bmatrix} 1 \\ 0 \end{bmatrix}$, and $\boldsymbol{C}=\begin{bmatrix} 1 & 0 \end{bmatrix}$.

3.2 Objective function and constraints

From the perspective of extending the life of the ESS, the energy storage output is reduced while satisfying the tracking plan, and the SOE converges to the ideal value by introducing the storage SOE variation into the optimization process to improve the adaptability of ESS to future wind power changes. Therefore, the objective function is established with the deviation of grid-connected power from the planned output and the minimum deviation of ESS remaining capacity from the ideal value, as:

$$\begin{aligned} \min J = \beta \sum_{k=1}^{N} \left| P_g^2(i+k|i) - P_a^2(i+k|i) \right| + \\ \alpha \sum_{k=1}^{N} \left| C_{SOE}^2(i+k|i) - C_{ideal}^2 \right| \end{aligned} \tag{8}$$

where C_{ideal} denotes the ideal ESS residual capacity, which is 0.5 times the rated capacity, and α and β denote the weight coefficients with $\alpha+\beta=1$.

The following charging and discharging power and SOC constraints should also be satisfied along with the MPC rolling optimization objective function.

(1) ESS capacity constraints

Considering factors such as ESS service life and safety, the SOC should satisfy the inequality constraint equation of:

$$E_{SOC.\min} \leq E_{SOC}(i) \leq E_{SOC.\max} \tag{9}$$

where $E_{soc.min}$ and $E_{soc.max}$ are the lower and upper limits of ESS SOC, respectively.

(2) ESS power constraints

The unequal constraint condition of ESS charging power is:

$$0 < P_b(i) \leq \min\left\{ P_{rated}, \frac{(E_{SOC.\max} - E_{SOC}(i))C_{rated}}{T_c} \right\} \tag{10}$$

where P_{rated} is the rated power of the ESS.

The unequal constraint condition of ESS discharge power is:

$$\max\left\{-P_{\text{rated}}, \frac{(E_{SOC.\min}-E_{SOC}(i))C_{\text{rated}}}{T_{\text{c}}}\right\} \le P_{\text{b}}(i) < 0 \tag{11}$$

3.3 Energy storage target power solution based on MPC rolling optimization method

Using the MPC control principle and combining (7)–(11), the problem can be transformed into a quadratic programming form to obtain the sequence of control variables, i.e., the target power tracked by the ESS, in the present and future periods.

$\boldsymbol{x}(i)$ is the known actual state value at moment i. From (7), the state variable $\boldsymbol{x}(i+1)$ at moment $i+1$ can be obtained, and the state variable at moment $i+2$ can be further calculated by $\boldsymbol{x}(i)$, as:

$$\begin{aligned}\boldsymbol{x}(i+2) = \boldsymbol{A}^2\boldsymbol{x}(i) + \boldsymbol{AB}_1\boldsymbol{u}(i) + \boldsymbol{AB}_2\boldsymbol{r}(i) + \\ \boldsymbol{B}_1\boldsymbol{u}(i+1) + \boldsymbol{B}_2\boldsymbol{r}(i+1)\end{aligned} \tag{12}$$

By analogy, an expression for the state variables at each moment can be obtained from $\boldsymbol{x}(i)$, all consisting of the known state and perturbation quantities, and the control variables to be solved. Let the sequence of state variables, the sequence of control variables, and the sequence of input quantities be divided as shown as:

$$\boldsymbol{x}_i = \begin{bmatrix}\boldsymbol{x}(i+1)\\ \boldsymbol{x}(i+2)\\ \cdots\\ \boldsymbol{x}(i+k)\end{bmatrix}, \boldsymbol{u}_i = \begin{bmatrix}\boldsymbol{u}(i+1)\\ \boldsymbol{u}(i+2)\\ \cdots\\ \boldsymbol{u}(i+k-1)\end{bmatrix}, \boldsymbol{r}_i = \begin{bmatrix}\boldsymbol{r}(i+1)\\ \boldsymbol{r}(i+2)\\ \cdots\\ \boldsymbol{r}(i+k-1)\end{bmatrix} \tag{13}$$

As $\boldsymbol{x}(i) = \boldsymbol{x}_0$, Eq. (12) can be expanded as:

$$\boldsymbol{X}_i = \boldsymbol{G}\boldsymbol{x}_0 + \boldsymbol{I}_1\boldsymbol{U}_i + \boldsymbol{I}_2\boldsymbol{R}_i \tag{14}$$

where the matrices of the coefficients are

$$\begin{aligned}\boldsymbol{G} &= \begin{bmatrix}\boldsymbol{A}\\ \boldsymbol{A}^2\\ \cdots\\ \boldsymbol{A}^k\end{bmatrix}\\ \boldsymbol{I}_1 &= \begin{bmatrix}\boldsymbol{B}_1 & 0 & \cdots & 0\\ \boldsymbol{AB}_1 & \boldsymbol{B}_1 & \cdots & 0\\ \cdots & \cdots & \cdots & \cdots\\ \boldsymbol{A}^{k-1}\boldsymbol{B}_1 & \boldsymbol{A}^{k-2}\boldsymbol{B}_1 & \cdots & \boldsymbol{B}_1\end{bmatrix}\\ \boldsymbol{I}_2 &= \begin{bmatrix}\boldsymbol{B}_2 & 0 & \cdots & 0\\ \boldsymbol{AB}_2 & \boldsymbol{B}_2 & \cdots & 0\\ \cdots & \cdots & \cdots & \cdots\\ \boldsymbol{A}^{k-1}\boldsymbol{B}_2 & \boldsymbol{A}^{k-2}\boldsymbol{B}_2 & \cdots & \boldsymbol{B}_2\end{bmatrix}\end{aligned} \tag{15}$$

Through matrix operations, all state variables in the optimization objective can be represented by control variables. Since the constant terms are not involved in the optimization and can thus be omitted, the objective function can be transformed into the standard quadratic programming form, as:

$$\min J = \frac{1}{2}\boldsymbol{U}_i^{\text{T}}\boldsymbol{H}\boldsymbol{U}_i + \boldsymbol{U}_i^{\text{T}}\boldsymbol{f} \tag{16}$$

where $\boldsymbol{H}$ and $\boldsymbol{f}$ are the quadratic term and primary term parameter matrices of the control variable that need to be solved, respectively.

The optimal sequence of control variables $\boldsymbol{U}_i$ that satisfies the optimization conditions and constraints, i.e., the storage tracking target power $P_{\text{b}}(i)$, $P_{\text{b}}(i+1)\ldots P_{\text{b}}(i+k)$, can be obtained by mathematical solutions. In theory, if the real system model aligns perfectly with the established mathematical model and the predictions are highly accurate, substituting the control sequence into the actual system should yield results consistent with the theoretically predicted state variables. However, various factors, such as model inaccuracies and disturbances, necessitate the use of rolling optimization to enhance control precision. When determining the optimal power storage target, it is essential to recognize that prediction information closer to the current time tends to be more accurate. Therefore, during each optimization step, only the first element of the sequence is chosen for controlling the system. As time progresses, at each moment, the state sequence is refreshed for prediction, and this process is repeated iteratively to correct errors that may have accumulated during the control process, ultimately leading to improved control accuracy.

4 Weight coefficient adjustment based on two-layer fuzzy control

The MPC rolling optimization objective function was defined in Sect. 3 taking into account the multi-objective optimization problem in which the deviations of grid-connected power from the planned output capacity and ESS remaining capacity from the ideal value are minimized. In the optimization process, optimizing the ESS output capacity depends entirely on the SOE. Therefore, in this section, the relationship between the ESS output capacity C_{SOE} and the dynamic regulation coefficient α is calculated by designing a two-layer fuzzy controller. The ESS operating state and grid-connected power are determined by adjusting the weights of the two optimization parts.

4.1 Weight coefficient analysis

To further analyze the influence of the weight coefficients on the objective function, we make $N=1$ in (8) and derive the derivative for J. Letting the derivative equal 0 allows for finding the ESS output power with the smallest objective function at the moment $i+1$, i.e.:

$$P_{\mathrm{b}}(i+1) = \frac{T_{\mathrm{c}}\alpha\left[C_{\mathrm{SOE}}(i) - C_{\mathrm{ideal}}\right] - \beta\left[P_{\mathrm{g}}(i) - P_{\mathrm{a}}(i)\right]}{T_{\mathrm{c}}\alpha + \beta} \tag{17}$$

As can be seen from (17), the ESS output power is controlled by α such that the larger α is, the closer the ESS residual capacity is to the ideal value, but the less effective the tracking plan curve is. On the contrary, if α is smaller, the tracking effect is better, but it could make the SOC over-bound. Therefore, the following method is used here to dynamically adjust α in real-time.

(1) At time $i+1$, when the predicted ultra-short-term wind power exceeds the upper or lower limits of the planned deviation band, the combined output of wind-storage should be ensured to be within the allowable deviation band of tracking. At the same time, the first layer fuzzy controller is used to correct α to keep the SOC from exceeding the limit.

(2) At time $i+1$, when the ultra-short-term wind power prediction is within the tracking allowable deviation band, it balances the contradiction between the planned power deviation and the ESS limit overrun in the future rolling optimization period. It improves the ability of the combined wind-storage system to track deviations from future plans while ensuring ESS life. At this time, the second layer fuzzy controller is used to correct the charging and discharging power of the ESS, and the correction formula is given as:

$$P_{\mathrm{b}}'(i+1|i) = P_{\mathrm{b}}(i+1|i) + \Delta k \times \delta P_{\mathrm{p}}(i+1|i) \tag{18}$$

where $P_{\mathrm{b}}'(i+1|i)$ is the operation instruction after ESS correction at time $i+1$ and Δk is the correction coefficient.

4.2 First layer of fuzzy control

As the capacity and charge and discharge power of an ESS have certain ranges, if the SOC and charge and discharge power exceed their allowable ranges, the service life of the ESS can be seriously affected. Based on this, a first layer fuzzy controller is used to adjust the charging and discharging power of the ESS to maintain the SOC within the allowed working range. The fuzzy controller is designed as double-input and single-output, i.e., the inputs are the energy storage output $P_{\mathrm{b}}(i)$ and SOC at time i, and the output is α. The fuzzy control input and output membership functions are shown in Fig. 5.

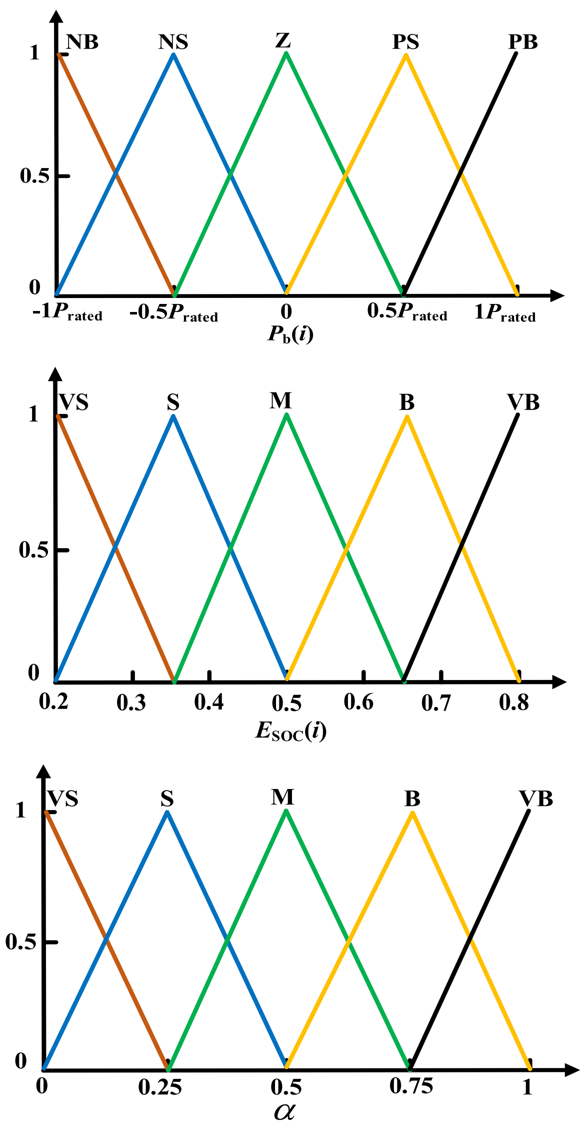

Fig. 5 Membership function of the first layer fuzzy controller

The universe of fuzzy control input variable $P_{\mathrm{b}}(i)$ is $[-1,1]$, and the fuzzy set is {NB,NS,Z,PS,PB}, which sequentially represent values that are negative large, negative small, zero, positive small, or positive large. The universe of $E_{\mathrm{soc}}(i)$ is [0.2,0.8], and the fuzzy set is {VS,S,M,B,VB}, which in turn sequentially represent values that are small, slightly small, slightly large, or large. The domain of fuzzy control output variable α is [0,1], and the fuzzy set is {VS,S,M,B,VB}, which sequentially represent values that are very small,

Table 1 The first layer of fuzzy control rules

$E_{SOC}(i)$	$P_b(i)$				
	PB	PS	Z	NS	NB
VS	VB	VB	B	M	M
S	B	B	M	M	S
M	S	VS	VS	VS	S
B	S	M	M	B	B
VB	M	M	B	VB	VB

small, moderate, large, or very large. The first layer fuzzy control rules are shown in Table 1.

4.3 Second layer fuzzy control

Based on the ultra-short-term wind power forecast value and the wind power plan value, the future SOE is evaluated, and then the charging and discharging are carried out in advance to improve the ESS's ability to track deviations from the future plan. The ESS off-limit power $W(i+k)$ and the planned power deviation $P_d(i+k)$ at each sampling point during the rolling optimization period are calculated as:

$$W(i+k) = \begin{cases} (E_{\mathrm{SOC}}(i+k) - E_{\mathrm{SOC.\,max}}) \times C_{\mathrm{rated}} \\ \quad E_{\mathrm{SOC}}(i+k) > E_{\mathrm{SOC.\,max}} \\ (E_{\mathrm{SOC.\,min}} - E_{\mathrm{SOC}}(i+k)) \times C_{\mathrm{rated}} \\ \quad E_{\mathrm{SOC}}(i+k) < E_{\mathrm{SOC.\,min}} \end{cases} \tag{19}$$

$$P_{\mathrm{d}}(i+k) = P_g(i+k) - P_a(i+k) \tag{20}$$

where $k=1,2,\ldots,N$ and N takes the value of 8. The covariance and correlation coefficients of the off-limit power and planned power deviations calculated from historical data are less than 0. It can be concluded that W and P_d are negatively correlated, and the contradiction factor F of the two variables W and P_d can be constructed by the following method.

First, the matrix is constructed through:

$$h_{ij} = \frac{1}{2}\left(\frac{1}{q}\sum_{j=1}^{q} d_{ij}^2 + \frac{1}{q}\sum_{i=1}^{q} d_{ij}^2 - d_{ij}^2 - I\right) \tag{21}$$

$$I = \frac{1}{q^2}\sum_{i=1}^{q}\sum_{j=1}^{q} d_{ij}^2 \tag{22}$$

$$d_{ij}^2 = \sum_{r=1}^{l} \left(z_{ir} - z_{jr}\right)^2 \tag{23}$$

where d_{ij}^2 denotes the square of the Euclidean distance of the i^{th} and j^{th} objects in matrix $\boldsymbol{Z}$, and $\boldsymbol{Z}$ is composed of the off-limit power and the planned power deviation. q is the number of rows in $\boldsymbol{Z}$ ($q=2$), and l is the number of columns in $\boldsymbol{Z}$ ($l=8$). z_{ir} is the element in row i and column r of $\boldsymbol{Z}$, while h_{ij} is the element of matrix $\boldsymbol{H}$.

After the eigenvalue decomposition of $\boldsymbol{H}$, the following is obtained:

$$\boldsymbol{H} = \boldsymbol{U}\boldsymbol{V}\boldsymbol{U}^{\mathrm{T}} \tag{24}$$

where $\boldsymbol{U}$ is the matrix with corresponding eigenvectors as columns and $\boldsymbol{V}$ is the diagonal matrix generated by the eigenvalues of $\boldsymbol{H}$. Then the contradiction factor F for the two variables W and P_d can be expressed by:

$$F = \boldsymbol{U}\sqrt{\boldsymbol{V}} \tag{25}$$

A very large F indicates that the ESS is overproducing in the future rolling optimization period, i.e., E_{SOC} has exceeded $E_{SOC.max}$ and the ESS should be discharged in advance. If F is very small, it means that the ESS has insufficient ability to track the planned output in the future rolling optimization period, i.e., E_{SOC} is lower than $E_{SOC.min}$, and the ESS needs to be charged in advance. If the spear F is moderate, the ESS is charged and discharged according to the original instructions. The input quantities of the second layer fuzzy controller are F and $P_b(i)$, and the output quantity is Δk. The fuzzy control input and output membership functions are shown in Fig. 6.

The universe of fuzzy control input variable $P_b(i)$ is [-1,1], and the fuzzy set is {L,LM,M,MH,H}, which sequentially represent values that are negative large, negative small, zero, positive small, or positive large. The universe of F is [-0.2,0.2], and the fuzzy set is {VS,S,B,VB}, which sequentially represent values that are small, slightly small, slightly large, or large. The universe of fuzzy control output variable Δk is [-1,1], and the fuzzy set is {NB,PB,N,Z,P,PH,NH}, which sequentially represent minimum, small, slightly small, moderate, slightly large, large, or maximum values. The fuzzy control rules are shown in Table 2, and Fig. 7 shows the specific process of the proposed control strategy.

5 Simulation analysis of numerical examples

The example scenario is based on the measured wind power data of a wind farm with an installed capacity of 50 MW, and the experiments are conducted to simulate integrated control in the combined wind-storage power generation system, as shown in Fig. 8.

The topological structure, system functions, and secondary parameters of the simulation platform refer to the

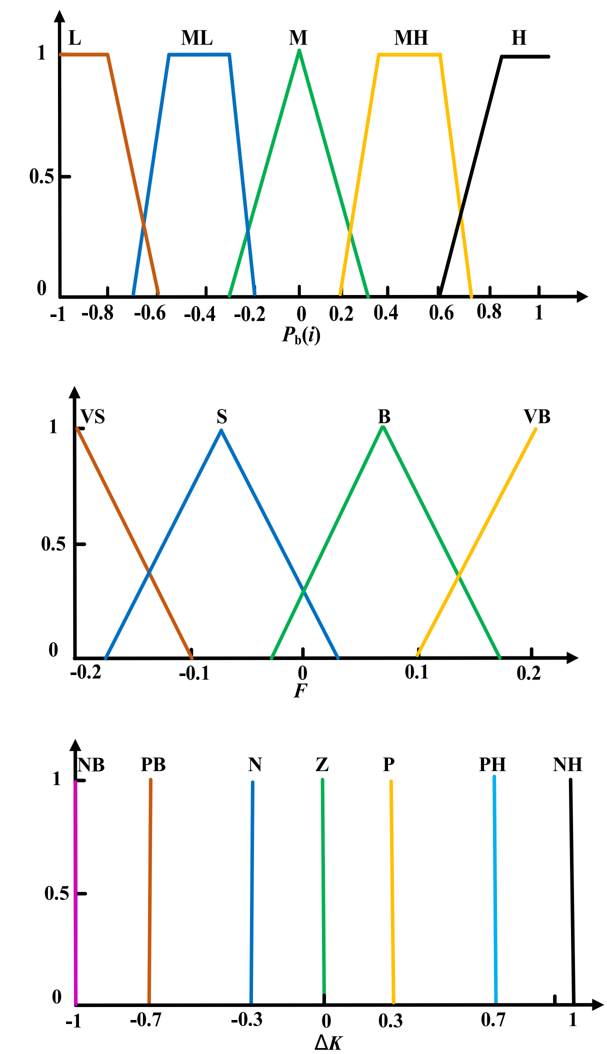

Fig. 6 Membership function of the second layer fuzzy controller

Table 2 The second layer of fuzzy control rules

F	$P_b(i)$				
	L	**LM**	**M**	**MH**	**H**
VS	NB	PB	P	NH	P
S	PB	N	Z	PH	Z
B	P	PH	Z	N	PB
VB	PH	NH	PB	PB	NB

actual engineering design, as shown in Fig. 9. The platform consists of an energy storage station energy management system, a wind farm SCADA system, a reactive power compensation monitoring system, a booster-station integrated automation system, and a system for the integrated intelligent monitoring of automatic power generation, voltage control, etc.

In this paper, the simulation parameters are mainly set by referring to the methods in [38] and [39]. In real-world engineering applications within China's power grid, the planned power generation curve is evaluated at 5-min intervals. Therefore, we also opt for a 5-min sampling period. Table 3 lists the main wind farm and ESS parameter settings. To illustrate the feasibility and superiority of the proposed control strategy (Scheme 4), it is compared with MPC control Schemes 1, 2 and 3, and Table 4 shows the settings of the four control methods.

5.1 Evaluation index

The advantages and disadvantages are evaluated based on the following four indicators: power prediction accuracy P_{re}, maximum tracking deviation $P_{\mathrm{d.max}}$, ESS dead time T_{d}, and ESS output coefficient C_{b}. Each of the indicators is descripted as follows.

(1)(1) Power prediction accuracy P_{re}

$$P_{re}=\left(1-\frac{\sqrt{\frac{1}{n}\sum_{i=1}^{n}\left[P_w(i)-P_p(i)\right]^2}}{Cap}\right)\times 100\% \tag{26}$$

where n is the number of samples, and Cap is the start-up capacity of the wind farm.

(2)(2) Maximum tracking deviation $P_{\mathrm{d.max}}$

$$P_{d.max}=\max\left|P_{\mathrm{g}}(i)-P_{\mathrm{p}}(i)\right| \tag{27}$$

where T_{d} is the time when the energy storage SOC exceeds the set safety threshold.

(3)(3) ESS dead time T_{d}

$$T_{\mathrm{d}}=T_{\mathrm{s}}\times\sum_{i=0}^{N-1}\left[h\left(\frac{E_{\mathrm{SOC}}(i)}{E_{\mathrm{SOC.\,min}}}\right)\bigcup h\left(\frac{E_{\mathrm{SOC.\,max}}}{E_{\mathrm{SOC}}(i)}\right)\right]$$
$$h(x)=\begin{cases}1, x\geq 1\\ 0, x<1\end{cases} \tag{28}$$

where T_{d} is the time when the energy storage SOC exceeds the set safety threshold.

(4)(4) ESS output coefficient C_{b}

$$C_b=\sqrt{\frac{1}{T-1}\sum_{i=1}^{T-1}\left[E_{\mathrm{SOC}}(i)-0.5\right]^2} \tag{29}$$

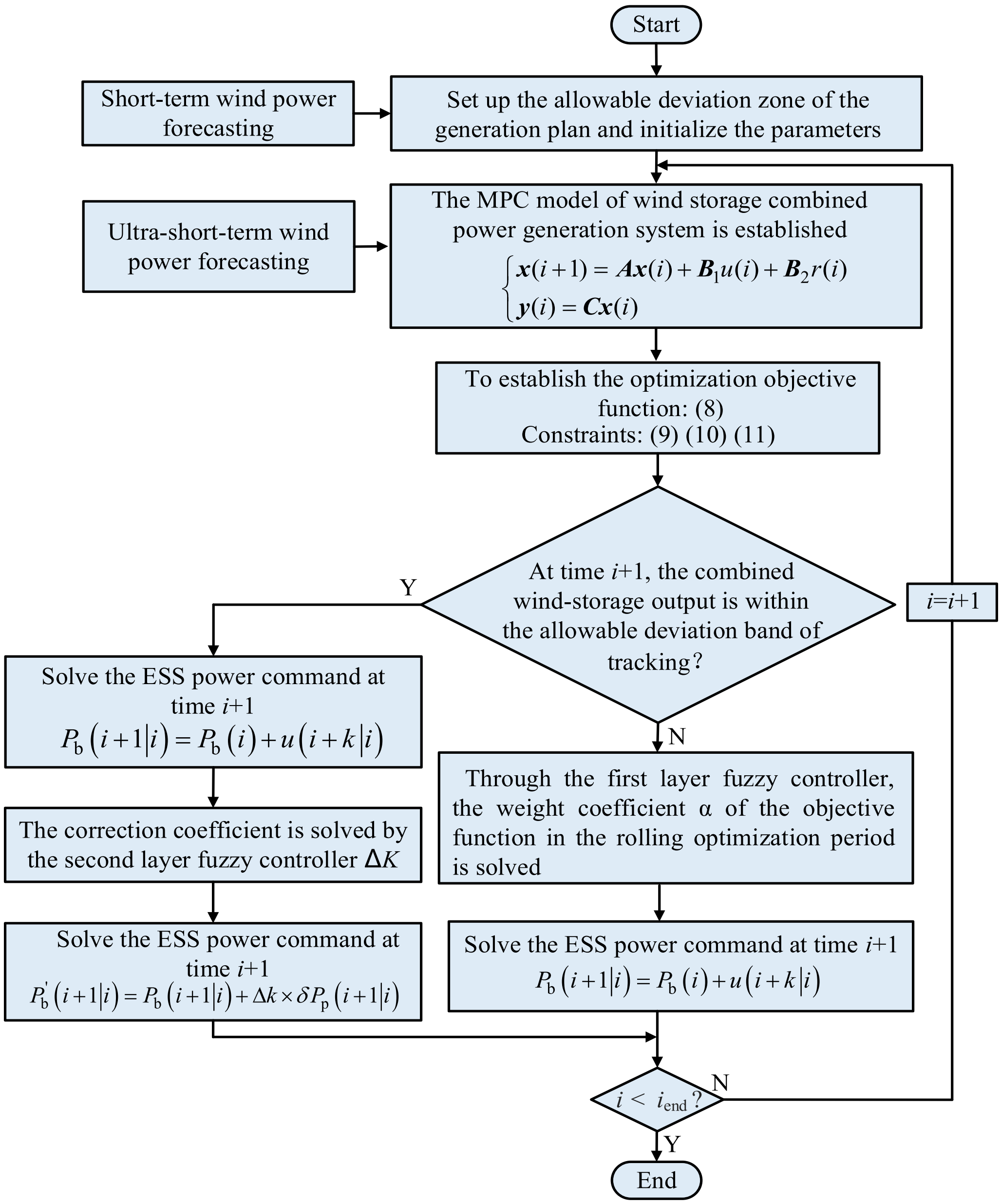

Fig. 7 Control flowchart

where T is the number of sampling periods in the energy storage output cycle. The smaller the value of C_b, the larger the output capacity.

5.2 Analysis of simulation results

The curves of the actual and planned wind power values selected in this paper are shown in Fig. 10. Taking the planned wind power in Fig. 10 as a reference, Fig. 11 displays the effect of the power generation planning curves of the wind-storage joint output tracking for the four control methods, and Table 5 shows the evaluation indices for the different control schemes.

As can be seen from Fig. 11, Schemes 1, 2 and 3 can largely ensure the joint output of wind-storage to be within the allowable deviation band of tracking for most of the time, while Scheme 4 fully meets the requirements. Table 5 shows that, compared to without energy storage, the prediction accuracies of the four control schemes with energy storage increase by 10.43%, 5.35%, 8.32%, and 11.31%, respectively, while the maximum tracking

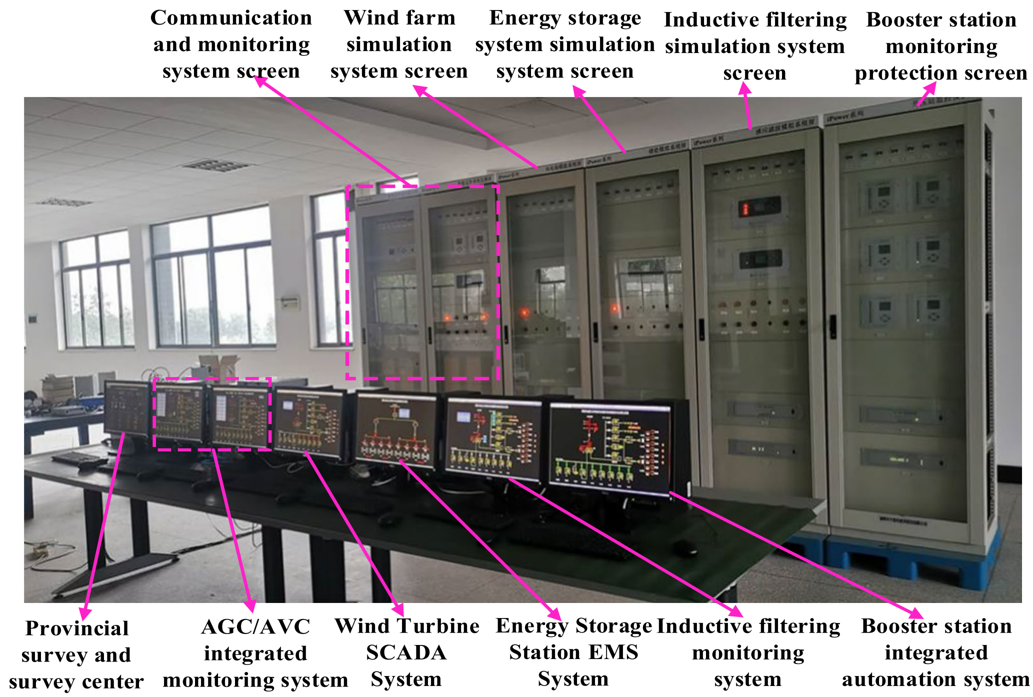

Fig. 8 Simulation test platform

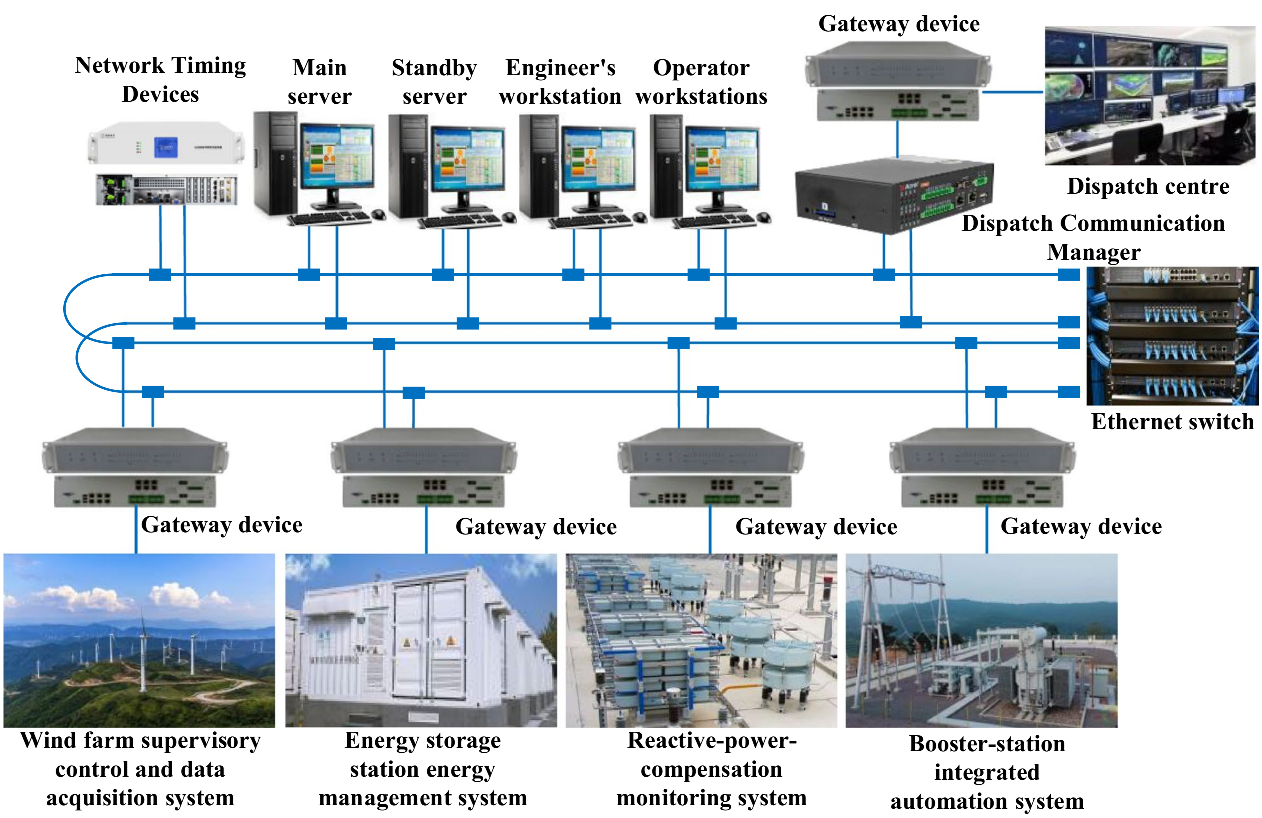

Fig. 9 Simulation platform network topology structure diagram

Table 3 Simulation parameters

parameters	Symbol	Value & Units
Installed capacity of wind farms	$C_{install}$	50 MW
Cycle of control	T_c	5 min
Rated capacity of ESS	C_{rated}	20 MW·h
Rated power of ESS	P_{rated}	10 MW
The deviation band sets the coefficient	δ	0.2
Sampling time	T_s	5 min
Upper limit of ESS state of charge	$E_{SOC.max}$	0.85
Lower bound of ESS state of charge	$E_{SOC.min}$	0.15

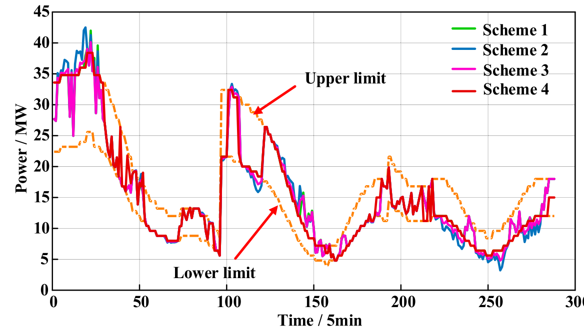

Fig. 11 Combined output curves of wind-storage with different control schemes

Table 4 Four different control schemes

Control scheme	Setup mode	Principle of optimization
Scheme 1	$\alpha=0$	The tracking plan has the smallest deviation
Scheme 2	$\alpha=1$	The deviation of the residual capacity of ESS from the ideal value is minimal
Scheme 3	–	MPC method for minimum output of ESS
Scheme 4	Dynamic adjustment α、Δk	The optimization method proposed in this paper

Table 5 Evaluation indices

Control scheme	P_{re}/%	$P_{d.max}$/MW	T_d/min	C_b
Without ESS	84.73	15.29	–	–
Scheme 1	93.57	9.97	180	0.226
Scheme 2	89.26	12.50	0	0.134
Scheme 3	91.39	9.11	55	0.197
Scheme 4	94.31	6.41	0	0.145

deviations decrease by 34.79%, 18.25%, 40.41%, and 58.08%, respectively. In summary, Scheme 4 has the best tracking effect, followed by Schemes 1, 3 and then 2.

The energy storage SOC variation curves in Fig. 12 show that Scheme 1 ESS is in a high energy state during the two time periods of 80–200 min and 710–850 min. This decreases its charging capacity. Table 5 also shows that Scheme 1 ESS dead time is as long as 170 min, and the capacity coefficient is 0.226. These do not support the ESS for tracking the planned capacity in the future. Scheme 2 takes the minimum deviation of ESS remaining capacity from the ideal value as the optimization target, and the SOC change curve is gradually adjusted toward 0.5. Although the ESS overrun limit is avoided, the tracking effect is poor. Figure 12 shows that the Scheme 3 ESS is in a high energy state during the time period of 145–200 min, which decreases its charging capacity. Table 5 also shows that Scheme 3 ESS dead time is 55 min, and the capacity coefficient is 0.197. These reduce the ability of ESS to track planned power output. Combined with the ESS power in Fig. 13, Scheme 4 improves the ability of the ESS to track the future planned curve by dynamically adjusting the weighting coefficient and charging and discharging in advance. Compared with Scheme 1,

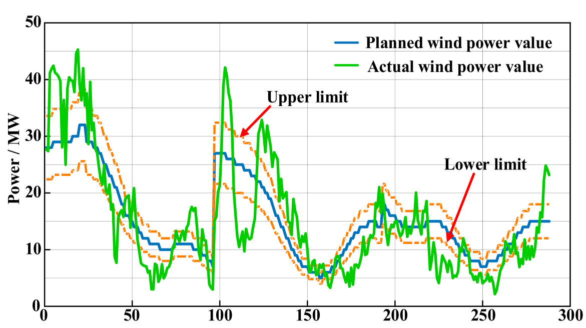

Fig. 10 Wind power actual output and planned output curve

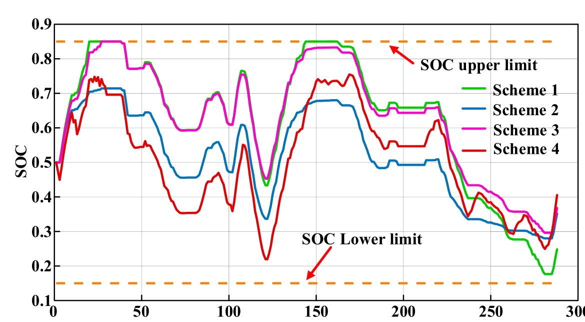

Fig. 12 SOC variation curves for the different control schemes

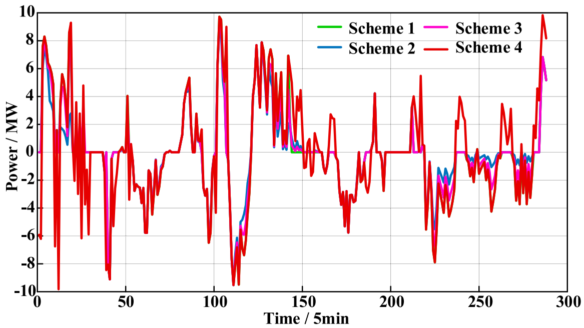

Fig. 13 ESS output curves for the different control schemes

Scheme 4 reduces the dead time and extends the service life of the ESS while improving the tracking of the planned curve. Compared with Scheme 2, Scheme 3 ESS output capacity is slightly reduced, but the ability to track the wind power planning curve is greatly improved. Compared with Scheme 3, Scheme 4 reduces the dead time and output coefficient while improving the tracking of the planned curve. Therefore, compared with Schemes 1, 2 and 3, the proposed method effectively balances the conflict between energy storage crossing limit and wind power plan tracking, and verifies the superiority of the proposed method.

5.3 Parameter analysis

In the process of constructing the proposed method, the determined rated power P_{rated}, rated capacity C_{rated}, and the size of the ESS deviation band setting coefficient δ have great impact on the tracking effect. Therefore, it is necessary to analyze the influence of relevant parameter changes on the control effect of the proposed method.

(1)(1) Influence of ESS power rating

For the ESS rated capacity $C_{\text{rated}} = 20$ MW·h and the deviation band set coefficient $\delta = 0.2$, the change rule of the evaluation index of each control scheme with different power ratings of ESS is compared, as shown in Fig. 14.

From Fig. 14, it is seen that ESS dead time and output coefficient are less affected by the rated power in Schemes 2 and 4, but more affected in Scheme 1. Compared with Scheme 1, the tracking effect of Scheme 4 is better when the rated ESS power is greater than 6.5 MW. Compared with Scheme 2, although the output capacity of Scheme 4 is slightly lower, its power prediction accuracy is much higher. Compared with Scheme 3, Scheme 4 also has better tracking effect and ESS output capacity. Therefore, as the rated power of ESS increases, the tracking effects of the four control schemes become better, while the control effect of Scheme 4 is the best.

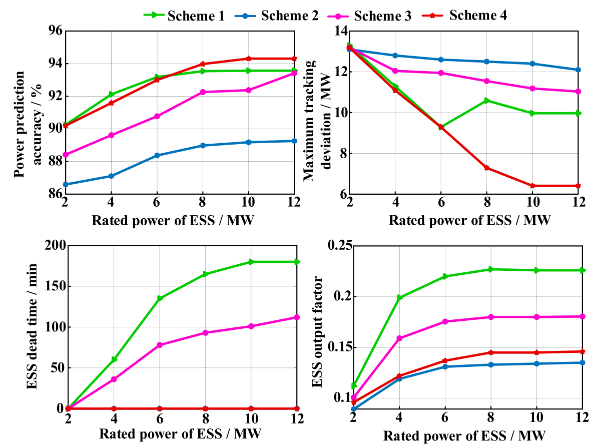

Fig. 14 Curves of the evaluation indices with different rated powers

(2)(2) Impact of ESS rated capacity

For the ESS rated power $P_{\text{rated}} = 10$ MW and the deviation band coefficient of $\delta = 0.2$, Fig. 15 shows the change rules of the evaluation indices for each control scheme with different rated ESS capacities.

As is seen from Fig. 15, as the ESS rated capacity increases, its dead time decreases substantially and the output capacity also decreases for the four control schemes. Compared with Schemes 1, 2 and 3, Scheme 4 has the best tracking effect, mainly because it considers the influence of the current ESS residual capacity on the future tracking ability and ensures that the ESS charging and discharging ability can cope with possible future wind power schedule deviations. That is, the proposed control method can appropriately reduce the required ESS capacity.

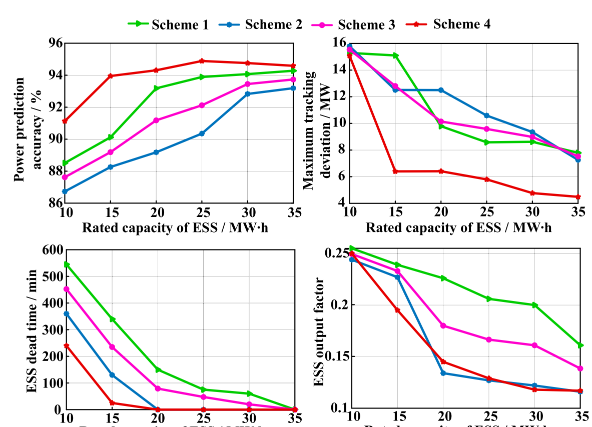

Fig. 15 Curve of the evaluation index with different rated capacities

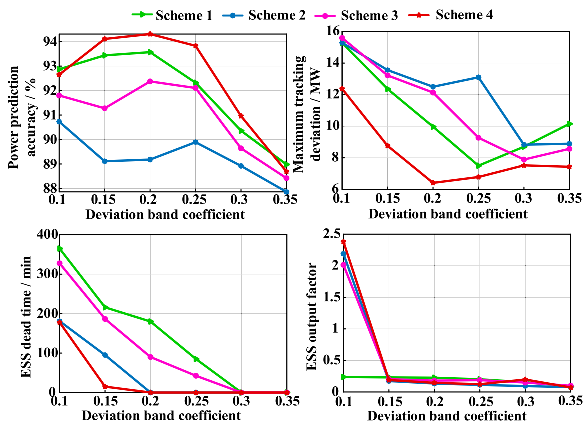

Fig. 16 Evaluation index curves with different deviation band coefficients

(3)(3) Impact of the deviation band setting coefficient

For ESS rated power of $P_{\text{rated}}=10$ MW and rated capacity of $C_{\text{rated}}=20$ MW·h, the change rule of the evaluation index of each control scheme with different deviation band coefficients is compared, as shown in Fig. 16.

With increasing deviation band coefficients, the requirement of tracking wind power plan output is relaxed, which reduces the ESS charging and discharging energy. The ESS dead time and output coefficient presented in Fig. 16 show that the tracking is worsened with each of the three control schemes, although wind power prediction accuracy and maximum tracking deviation show that Scheme 4 is still better than Schemes 1, 2 and 3. Therefore, the proposed method is superior.

6 Conclusion

In this paper, a power control strategy based on model prediction and double-layer fuzzy control is proposed for a combined wind-storage system to track wind power plan output that not only tracks wind power plan deviations but also increases the ESS's ability to track future plan deviations. From the findings, we can draw the following conclusions.

(1) An objective function is proposed to minimize the deviation of grid-connected power from the planned output, and the deviation of ESS remaining capacity from the ideal value. At the same time, a method of using the first layer of fuzzy controller is proposed to correct the weight coefficients of the objective. Compared with Schemes 1, 2 and 3, the power prediction accuracy in Scheme 4 is increased by 97.43%, 96.55%, and 93.75%, respectively. Compared with Schemes 1 and 3, Scheme 4 reduces the dead time by 180 min and 55 min, respectively. Thus, the proposed method reduces the dead time and extends the service life of the ESS while improving the tracking of the planned curve.

(2) Statistical factor analysis theory is used to construct the contradictory factors between the two variables of ESS off-limit power and planned power deviation in the future optimization period. A method of using the second layer of fuzzy control rules is proposed to correct the charging and discharging power of the ESS. Compared with Schemes 1, 2 and 3, the maximum tracking deviation in Scheme 4 is decreased by 35.71%, 48.72%, and 29.64%, respectively. Compared with Scheme 1 and 3, the ESS output coefficient in Scheme 4 is decreased by 35.84% and 26.40%, respectively. Hence, charging and discharging are carried out in advance to improve the utilization level of the ESS and the ESS's ability to track deviations from the future plan.

(3) The effectiveness of the proposed control strategy is affected by the ESS's rated power, rated capacity and deviation band setting coefficient. However, under the same conditions, the comprehensive index of the proposed control strategy is better than the indices under Schemes 1, 2 and 3, and effectively offsets the conflict between the planned wind power output tracking and the excess of the ESS. The proposed control method can appropriately reduce the required ESS capacity, so as to improve ESS economy.

Acknowledgements
Not applicable.

Author contributions
All authors contributed to the research, read and approved the manuscript. Formal analysis: TGY; Investigation: JYY; Supervision: L. F. LUO; Writing-original draft: J. Y. YANG; Writing-review and editing: L. F. LUO; Data curation: LI PENG. All authors have readand approved the fnal manuscript.

Funding
This work was supported by the Major Science and Technology Project of Hunan Province (2020GK1013); Project of Natural Science Foundation of Hunan Province (2023JJ50344); Project of Educational Commission of Hunan Province (22C0512).

Availability of data and materials
Please contact author for data and material request.

Declarations

Competing interests
The authors declare that they have no known competing fnancial interests or personal relationships that could have appeared to infuence the work reported in this paper.

Received: 3 January 2023 Accepted: 2 November 2023
Published online: 14 November 2023

References

1. Lin, Z. J., Chen, H. Y., Wu, Q. W., et al. (2020). Mean-tracking model based stochastic economic dispatch for power systems with high penetration of wind power. *Energy, 193*(5), 1–13.
2. Su, Y., & Teh, J. (2023). Two-stage optimal dispatching of AC/DC hybrid active distribution systems considering network flexibility. *Journal of Modern Power Systems and Clean Energy, 33*(1), 52–65.
3. Dui, X. W., Zhu, G. P., & Yao, L. Z. (2018). Two-stage optimization of battery energy storage capacity to decrease wind power curtailment in grid-connected wind farms. *IEEE Transactions on Power Systens, 33*(3), 3296–3305.
4. Li, X. J., Ma, R., Gan, W., et al. (2022). Optimal dispatch for battery energy storage station in distribution network considering voltage distribution improvement and peak load shifting. *Journal of Modern Power Systems and Clean Energy, 10*(1), 131–139.
5. He, G. N., Chen, Q. X., Kang, C. Q., et al. (2016). Optimal bidding strategy of battery storage in power markets considering performance-based regulation and battery cycle life. *IEEE Transactions on Smart Grid, 7*(5), 2359–2367.
6. Jiang, Q., & Hong, H. (2013). Wavelet-based capacity configuration and coordinated control of hybrid energy storage system for smoothing out wind power fluctuations. *IEEE Transactions on Power Systems, 28*(2), 1363–1372.
7. Siqueira, D., Maria, S. L., & Wei, P. (2021). Control strategy to smooth wind power output using battery energy storage system: A review. *Journal of Energy Storage, 35*, 102252–102263.
8. Guo, T. T., Liu, Y. B., Zhao, J. B., Zhu, Y. W., et al. (2020). A dynamic wavelet-based robust wind power smoothing approach using hybrid energy storage system. *International Journal of Electrical Power & Energy Systems, 116*, 105579.
9. Choopani, K., Effatnejad, R., & Hedayati, M. (2020). Coordination of energy storage and wind power plant considering energy and reserve market for a resilience smart grid. *Journal of Energy Storage, 30*, 101542–101550.
10. Teixeira, T. P., & Borges, C. L. T. (2021). Operation strategies for coordinating battery energy storage with wind power generation and their effects on system reliability. *Journal of Modern Power Systems and Clean Energy, 9*(1), 190–198.
11. Zhai, Y. J., Zhang, J. W., Tian, Z. W., et al. (2021). Reseaarch on the application of superconducting magenetic energy stogage in the wind power generation system for smoothing wind power fluctuations. *IEEE Transactions on Applied Superconductivity., 31*(5), 1–5.
12. Zhou, Y., Yan, Z., & Li, N. H. (2017). A novel state of charge feedback strategy in wind power smoothing based on short-term forecast and scenario analysis. *IEEE Transactions on Sustainable Energy, 8*(2), 870–876.
13. Barra, P. H. A., De Carvalho, W. C., Menezes, T. S., et al. (2021). A review on wind power smoothing using high-power energy storage systems. *Renewable & Sustainable Energy Reviews, 137*, 110455.
14. Dong, J. J., Gao, F., Guan, X. H., et al. (2017). Storage sizing with peak-shaving policy for wind farm based on cyclic Markov chain model. *IEEE Transactions on Sustainable Energy., 8*(3), 978–989.
15. Roy, P., Liao, Y., & He, J. B. (2023). Economic dispatch for grid-connected wind power with battery-supercapacitor hybrid energy storage system. *IEEE Transactions on Industry Applications, 59*(1), 1118–1128.
16. Guo, Z. J., Wei, W., Shahidehpour, M., et al. (2023). Two-timescale dynamic energy and reserve dispatch with wind power and energy storage. *IEEE Transactions on Sustainable Energy, 14*(1), 490–503.
17. Sewnet, A., Khan, B., Gide, I., et al. (2022). Mitigating generation schedule deviation of wind farm using battery energy storage system. *Energies, 15*(5), 1768.
18. Emara, D., Ezzat, M., Abdelaziz, A. Y., et al. (2021). Novel control strategy for enhancing microgrid operation connected to photovoltaic generation and energy storage systems. *Electronics, 10*(11), 1261.
19. Rong, S., Chen, X. G., Guan, W. L., et al. (2019). Coordinated dispatching stragery of multiple energy sources for wind power consumption. *Journal of Modern Power Systems and Clean Energy, 7*(6), 1461–1471.
20. Rayit, N. S., Chowdhury, J. I., & Balta-Ozkan, N. (2021). Techno-economic optimisation of battery storage for grid-level energy services using curtailed energy from wind. *Energy Storage, 39*, 102641.
21. Li, J. H., Wang, S., Ye, L., et al. (2018). A coordinated dispatch method with pumped-storage and battery-storage for compensating the variation of wind power. *Protection and Control of Modern Power Systems., 3*(1), 21–34.
22. Dhiman, H. S., & Deb, D. (2020). Wake management based life enhancement of battery energy storage system for hybrid wind farms[J]. *Renewable & Sustainable energy reviews, 130*, 109912.
23. Nguyen, C. L., & Lee, H. H. (2017). Optimal power control strategy for wind farm with energy storage system. *Journal of Electrical Engineering Technology, 12*(2), 726–737.
24. Moghaddam, I. N., Chowdhury, B. H., & Mohajeryami, S. (2018). Predictive operation and optimal sizing of battery energy storage with high wind energy penetration. *IEEE Transactions on Industrial Electronics, 65*(8), 6686–6692.
25. Li, Q., Choi, S. S., Yuan, Y., et al. (2011). On the determination of battery energy storage capacity and short-term power dispatch of a wind farm. *IEEE Transactions on Sustainable Energy, 2*(2), 148–158.
26. Shi, J., Wang, L., Le, W. J., et al. (2019). Hybrid Energy Storage System (HESS) optimization enabling very short-term wind power generation scheduling based on output feature extraction. *Applied Energy, 256*, 113915.
27. Zhang, X. S., Yuan, Y., Hua, L., et al. (2017). On generation schedule tracking of wind farms with battery energy storage systems. *IEEE Transactions on Sustainable Energy, 8*(1), 341–353.
28. Kani, S. A. P., Wild, P., & Saha, T. K. (2020). Improving predictability of renewable generation through optimal battery sizing. *IEEE Transactions on Sustainable Energy, 11*(1), 37–47.
29. Baker, K., Hug, G., & Li, X. (2016). Energy storage sizing taking into account forecast uncertainties and receding horizon operation. *IEEE Transactions on Sustainable Energy, 8*(1), 331–340.
30. Moghaddam, I. N., Chowdhury, B. H., & Mohajeryami, S. (2017). Predictive operation and optimal sizing of battery energy storage with high wind energy penetration. *IEEE Transactions on Industrial Electronics, 65*(8), 6686–6695.
31. Esmaeili S., Amini M., Khorsandi A., et al. (2021). Market-oriented optimal control strategy for an integrated energy storage system and wind farm. in *2021 29th Iranian Conference on Electrical Engineering (ICEE)*, Tehran, Iran, Islamic Republic of, 407–411.
32. Guo, T. T., Zhu, Y. W., Liu, Y. B., et al. (2020). Two-stage optimal MPC for hybrid energy storage operation to enable smooth wind power integration. *IET Renewable Power Generation, 14*(13), 2477–2486.
33. Sun, Y. S., Tang, X. S., Sun, X. Z., et al. (2019). Model predictive control and improved low-pass filtering strategies based on wind power fluctuation mitigation. *Journal of Modern Power Systems and Clean Energy, 7*(3), 512–524.
34. Long, B., Liao, Y., Chong, K. T., et al. (2021). Enhancement of frequency regulation in AC microgrid: A fuzzy-MPC controlled virtual synchronous generator. *IEEE Transactions on Smart Grid, 12*(4), 3138–3149.
35. Tang, L., Xu, W., Wang, X., Dong, D., et al. (2021). Weighting factors optimization of model predictive control based on fuzzy thrust constraints for lLinear induction machine. *IEEE Transactions on Applied Superconductivity, 31*(8), 1–5.
36. National Energy Board. NB/T10205-2019 Technical rules for wind power forecasting. Beijing: StandardPress of China, 2019
37. Oskouei, M. Z., & Yazdankha, A. S. H. (2017). The role of coordinated load shifting and frequency-based pricing strategies in maximizing hybrid system profit. *Energy, 135*(15), 370–381.
38. Zhang, F., Meng, K., Zhao, X., et al. (2017). Battery ESS planning for wind smoothing via variable-inteval reference modulation and self-adaptive SOC control strategy. *IEEE Transactions on Sustainable Energy, 8*(2), 695–707.
39. Shi J., Lee W. J., Liu X. F. (2017). Generation scheduling optimization of wind-energy storage system based on wind power output fluctuation featuers. in 2017 IEEE/IAS 53rd Industral and Commercial Power Systems Technical conference(I&CPS), Niagara Falls, ON, Canada, 1–7.

Jingyu Yang (1986-), male, He is currently pursuing the Ph.D. degree in electrical engineering with the College of Electrical and Information Engineering, Hunan University. His current research interests include power system informatization, intelligent algorithm, and renewable power generation.

Tongguang Yang (1974-), male, He is currently a professor working in the school of mechanical and electrical engineering, Hunan city university. His current research interests include the grid-connected inverters control for new energy, fault diagnosis for induction motor.

Longfu Luo (1962-), male, He is currently a Full Professor of electrical engineering with the College of Electrical and Information Engineering, Hunan University. His current research interests include the design and optimization of modern electrical equipment, the development of new converter transformer, and the study of corresponding new HVDC theories.

Li Peng (1987-), female, She works in the school of mechanical and electrical engineering, Hunan city university. Her current research fields include power system informatization, intelligent algorithm, and new energy.